Biochemistry

pubs.acs.org/biochemistry Article

Riboflavin Stabilizes Abasic, Oxidized G-Quadruplex Structures

Rodrigo Galindo-Murillo,[§] Lauren Winkler,[§] Jingwei Ma, Fatjon Hanelli, Aaron M. Fleming, Cynthia J. Burrows, and Thomas E. Cheatham, III*

Cite This: *Biochemistry* 2022, 61, 265−275 Read Online

ACCESS | Metrics & More | Article Recommendations | Supporting Information

ABSTRACT: The G-quadruplex is a noncanonical fold of DNA commonly found at telomeres and within gene promoter regions of the genome. These guanine-rich sequences are highly susceptible to damages such as base oxidation and depurination, leading to abasic sites. In the present work, we address whether a vacancy, such as an abasic site, in a G-quadruplex serves as a specific ligand recognition site. When the G-tetrad is all guanines, the vacant (abasic) site is recognized and bound by free guanine nucleobase. However, we aim to understand whether the preference for a specific ligand recognition changes with the presence of a guanine oxidation product 8-oxo-7,8-dihydroguanine (OG) adjacent to the vacancy in the tetrad. Using molecular dynamics simulation, circular dichroism, and nuclear magnetic resonance, we examined the ability for riboflavin to stabilize abasic site-containing G-quadruplex structures. Through structural and free energy binding analysis, we observe riboflavin's ability to stabilize an abasic site-containing G-quadruplex only in the presence of an adjacent OG-modified base. Further, when compared to simulation with the vacancy filled by free guanine, we observe that the free guanine nucleobase is pushed outside of the tetrad by OG to interact with other parts of the structure, including loop residues. These results support the preference of riboflavin over free guanine to fill an OG-adjacent G-quadruplex abasic vacancy.

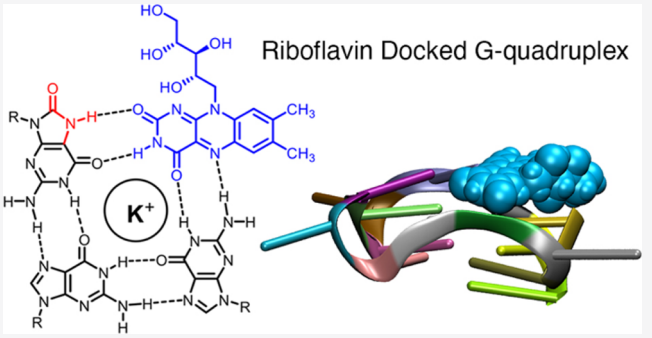

INTRODUCTION

DNA can fold into different biologically relevant structures such as the G-quadruplex, an alternative structure to the canonical B-DNA double helix that can have very high stability.[1] In DNA, G-quadruplexes are helical structures comprising stacks of at least two planar G-tetrads, where the four G-repeat sequences form the core of the G-quadruplex and may be flanked by 1−7 nucleotides.[1−3] Each G-tetrad consists of four guanines in a cyclic, Hoogsteen hydrogen-bonding arrangement.[4] The stability of this structure requires the presence of a monovalent cation between the quartets, such as K^+ or Na^+, for which K^+ ions have the greatest intracellular concentrations and result in the most stable folds.[5] Single-stranded, guanine-rich sequences can self-assemble and fold into G-quadruplex structures at physiological Na^+ and K^+ concentrations.[5] G-quadruplexes can be categorized by their topologies described as parallel, antiparallel, and hybrid depending on the relative directionality of the strands.[6,7] The G-quadruplex fold as a structural motif plays a critical role in several biological processes, and it also plays an important role in genomic regions such as gene promoters and telomeres.[5] The 3′ end of human telomeres is single-stranded and rich in guanine content with ∼100−200 nucleotides that serve as binding sites for many proteins.[8] This region has been observed to fold into G-quadruplexes in vivo.[3] Telomerase is an enzyme responsible for the maintenance of the length of telomeres and is overexpressed in 80−90% of cancer cells.[8,9] The formation of telomeric G-quadruplexes has been shown to inhibit telomerase activity from its end-capping functionality.[10,11] Subsequently, the formation and stability of G-quadruplexes inhibit cancer cell growth. Thus, the formation of stable G-quadruplex structures has emerged as a promising cancer therapy.[2,12,13]

One characteristic of these G-rich regions is their greater sensitivity to oxidation.[14−16] Of the four canonical bases, the guanine heterocycle is the most electron-rich, and therefore, it is the most susceptible to oxidation.[15,16] When guanine bases form a π-stacked conformation, such as in a G-quadruplex, the ionization potential of the 5′ most guanine is lowered.[14] The oxidation of guanine from naturally occurring inflammatory stress in the cell can lead to a consistent set of products including 8-oxo-7,8-dihydroguanine (OG), 2-iminohydantoin, spiroiminodihydantoin, 5-guanidinohydantoin, and imidazolone/oxazolone.[17,18] Recent studies have found that the oxidation of guanines in biologically relevant regions, such as

Received: September 8, 2021
Revised: January 12, 2022
Published: February 1, 2022

https://doi.org/10.1021/acs.biochem.1c00598
Biochemistry 2022, 61, 265−275

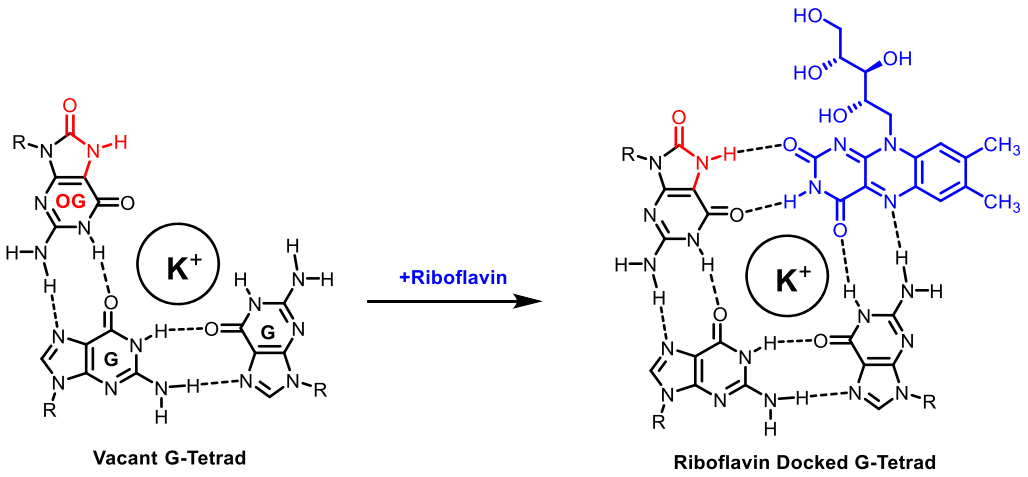

Figure 1. A vacant abasic G-tetrad with OG (red) in a G-quadruplex serves as a recognition site for riboflavin (blue). The predicted interaction of riboflavin (Fl, blue) hydrogen bonding with an OG residue (red) and the adjacent guanine.

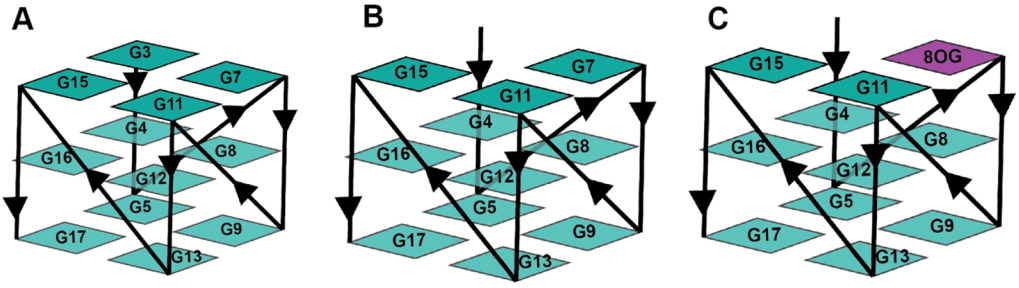

Figure 2. Schematic representation of the (A) WT parallel G-quadruplex structure, (B) abasic parallel G-quadruplex structure, referred to as 2DOR, and (C) abasic, oxidized parallel G-quadruplex structure referred to as 2DOR-8OG throughout this paper. The exact structure of the 8OG-modified base can be visualized in Figure 1.

gene promoters, can function as chemical markers for the modulation of gene expression.[19−22] The results of studies in model cells or organisms living in aerobic conditions have found OG to be the modification of the highest occurrence in the genome.[23,24] In addition to the oxidation of guanine to produce modified bases, these regions of genomic DNA are susceptible to becoming abasic sites due to a loss of the guanine base.[25] Typically, this loss of a base comes from the spontaneous hydrolysis of the *N*-glycosidic bond, resulting in depurination, or as intermediates in the DNA repair process.[26] The depurination of guanine to yield an abasic site greatly affects the stability of the G-quadruplex.[25,27] Though a G-quadruplex can be formed with an abasic site, abasic site-containing G-quadruplexes are significantly less stable based on thermodynamic studies.[27] With less stability, abasic site-containing G-quadruplexes in telomeres are more likely to unfold to their single-stranded form.[28] Interestingly, the abasic site in the G-quadruplex forms a vacancy that can serve as a docking site for a guanine nucleobase.[29−31] Therefore, the ability of a small molecule to interact with and stabilize telomeric quadruplexes is highly appealing.[2,28] The search for telomeric stabilizing binding agents has led to a number of discoveries including quinoline-based triazine compounds, acridine derivatives, perylene derivatives, and even organo-metallic complexes.[32−35] However, there has been an increased focus on molecules that could already be present in the cell. Riboflavin, known as vitamin B_2, is an essential molecule.[36] It acts as a precursor of the flavin mononucleotide and flavin adenine dinucleotide.[36] Structurally, riboflavin is a planar, heterocyclic molecule that is similar in structure to nucleobases; it has a complementary H-bonding for filling a vacancy in the G-quadruplex containing an OG, making it an excellent candidate to stabilize the modified G-quadruplex (Figure 1).[36]

In this work, we used molecular dynamics (MD) simulation, circular dichroism (CD), and NMR experiments to study the stabilization and interaction of riboflavin and the guanine nucleobase with damaged and native G-quadruplex structures. We look to identify (a) the influence of both riboflavin and the guanine nucleobase on an abasic G-quadruplex structure and (b) the effect of an OG modification on its interaction with the two ligands in an abasic quadruplex. Additionally, we compare the stabilizing effects and free energies of both riboflavin and a free guanine nucleobase from the potential of mean force estimations. Finally, we attempted to observe, without success likely due to the limited simulation time scale, an unbiased ligand recognition event of riboflavin at the abasic site vacancy in a G-quadruplex.

METHODS

MD Simulations. Riboflavin was built using GaussView[37] and optimized with DFT using M06-2x[38] and a 6-311(d,p) basis set; charges were calculated using HF/6-31G*[39] and adjusted using the restrained electrostatic potential methodology; the general AMBER force field was used to describe the molecule for the MD simulations.[40] The propeller-type parallel-stranded G-quadruplex structure with the sequence 5′-d(TTGGGTGGGTGGGTGGGT) modeled, referred to as

https://doi.org/10.1021/acs.biochem.1c00598
Biochemistry 2022, 61, 265−275

Table 1. Structural Difference Analysis Using Average Structures from Entire Aggregated Trajectories[a]

	entire G-quadruplex					tetrads				
rmsd (Å)	WT	2DOR	2DOR + docked	2DOR-OG	2DOR-OG + docked	WT	2DOR	2DOR + docked	2DOR-OG	2DOR-OG + docked
WT		1.2	2.4	1.6	1.3		0.4	2.0	0.7	0.6
2DOR	1.2		2.2	0.9		0.4		2.1	0.5	
2DOR + docked	2.4	2.2			2.1	2.0	2.1			1.9
2DOR-OG	1.6	0.9			1.3	0.7	0.5			1.8
2DOR-OG + docked	1.3		2.1	1.3		0.6		1.9	1.8	

[a]Differences between the two average structures are shown in Å. "Docked" refers to systems for which riboflavin is manually placed in the abasic site of the G-quadruplex. The columns on the left refer to rmsd analysis of the entire G-quadruplex structure, while the columns on the right refer to the rmsd of only the residues in the tetrad part of the structure, specifically residues 3−4, 7−9, 11−13, and 15−17. These data eliminate the potential influence from the loop regions of the G-quadruplex, which are known for their increased fluctuations.

wild-type (WT), was based on an average of 10 NMR structures (PDB: 2LK7)[41] and described using the OL15[42] force field. The G-quadruplex structure with an abasic site was created by replacing the first guanine in the top guanine tetrad with a 2-deoxyribose (referred to as 2DOR), specifically, d(TT-**2DOR**-GGTGGGTGGGTGGGT). The oxidized, abasic site-containing structure was created taking the 2DOR sequence and replacing the G7 residue in the top tetrad with an OG: d(TT-**2DOR**-GGT-**OG**-GGTGGGTGGGT), referred to as 2DOR-OG (Figure 2).

Parameters for OG were obtained from the Simmerling Lab;[43] the 2-deoxyribose molecule was built using the same methodology as the riboflavin molecule (parameters are available in the Supporting Information). All G-quadruplex structures were solvated in a cubic box using the TIP3P[44] water molecules. Potassium ions were added to neutralize the charge and an excess of KCl ions was added to reach an ∼200 mM concentration (estimated based on the initial volume) using the Joung−Cheatham ion model.[45] Minimization and equilibration protocols were followed as per our previous work.[46] After the initial equilibration, five independent copies (each with a different initial excess ion placement) of each of our WT controls and hand-docked riboflavin environments were run for ∼4.5 μs each at 300 K using the Berendsen thermostat for temperature control with a coupling value of 5.0.[47] Twenty independent copies (each with a different initial excess ion placement) of each of our free riboflavin and docked guanine nucleobase environments were run for ∼2 μs each under similar conditions. MD was performed using pmemd.-cuda GPU code from the AMBER 16 and AMBER 18 suite of programs.[48,49] Trajectory analysis was performed using CPPTRAJ v.18.00.[50] Quantum chemical calculations were performed using the D.01 version of Gaussian 09.[51] To manage the significant volume of MD simulation data, the analysis was performed by combining each of the five individual copies into an aggregated, water stripped, and root mean square-fitted trajectory. The complex of riboflavin with the G-quadruplex binding energies was computed using the molecular mechanics-Poisson−Boltzmann surface area (MM-PBSA) methodology using MMPBSA.py.[52] The free binding energies were calculated as

$$\Delta G_{\text{binding}} = \Delta G_{\text{complex}} - \Delta G_{\text{ligand}} - \Delta G_{\text{receptor}} \quad (1)$$

Then, the calculated free binding energies of the docked complexes were subtracted from the control complexes to find the change in the binding energy. This can be shown by the equation below

$$\Delta\Delta G = \Delta G_{\text{docked}} - \Delta G_{\text{control}} \quad (2)$$

Clustering analysis was performed using CPPTRAJ on every 10 frames. The DBSCAN clustering algorithm was used with a minimum of five points to form a cluster and 2 Å distance cutoff for each forming cluster. Scripts for performing the analyses are provided in the Supporting Information.

Experimental characterization of riboflavin docking into the vacancy of the OG containing a G-quadruplex was achieved using CD spectroscopy and ^{1}H NMR. The oligonucleotides were synthesized, purified, and characterized as previously described.[53] For the CD studies, the G-quadruplexes at 10 μM in 200 μL were first annealed by heating to 90 °C and slowly cooling to room temperature in 20 mM potassium phosphate buffer (pH 7.4) with 20 mM KCl present. Riboflavin was added at 100 μM, and the sample was allowed to incubate for 30 min before analysis. The CD spectra were recorded at 20 °C by scanning from 320 nm down to 220 nm, and the ellipticity values were normalized to the molar ellipticity values for the plots presented. For the ^{1}H NMR studies, the G-quadruplexes were annealed the same way in 20 mM potassium phosphate buffer (pH 7.0) and 30 mM KCl in a 9:1 H_2O/D_2O solvent at a volume of 300 μL. The riboflavin stock was titrated from 0.3 to 1.3 equiv by a bolus addition and waiting 30 min at 22 °C before recording the ^{1}H NMR spectra using the Watergate solvent suppression pulse sequence. The oligomers for thermal melting (T_m) analysis were first annealed at a 10 μM DNA concentration, and then T_m values were determined in 20 mM potassium phosphate buffer (pH 7.4) with 20 mM KCl, and either 0 or 100 μM riboflavin was present. The samples were placed in a quartz T_m analysis cuvette that was placed in a temperature-regulated UV−vis spectrometer followed by thermal equilibration at 20 °C before the commencement of the experiment. The thermally induced denaturation of the G4s was monitored at 295 nm by heating the sample from 20 to 100 °C at a ramp rate of 0.5 °C/min followed by a 60 s equilibration and then measuring the absorbance value at 295 nm. The absorbance data collected were background-subtracted, and then T_m values were determined using Shimadzu's T_m analysis software.

RESULTS AND DISCUSSION

Overall, we obtained an aggregated 2.8 ms of MD trajectory data. With these data, we were able to answer key questions pertaining to the stabilization of abasic G-quadruplex structures. This included the influence of an OG near the abasic site and the comparison of riboflavin to a bound guanine nucleobase.

Riboflavin Stabilizes the Damaged G-Quadruplex Structure. Our first goal was to observe the inherent stability or instability of the damaged G-quadruplex structures both

https://doi.org/10.1021/acs.biochem.1c00598
Biochemistry 2022, 61, 265−275

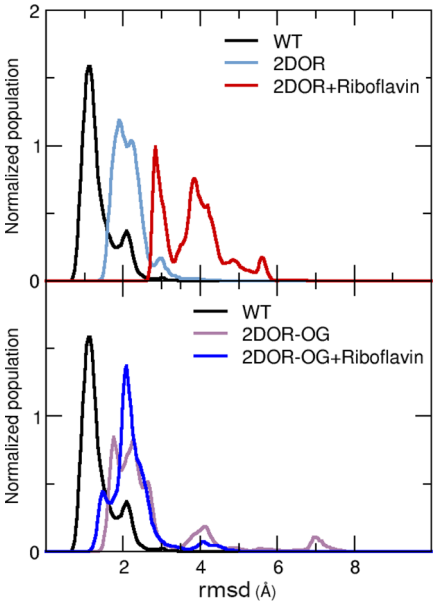

Figure 3. Histograms depicting the rmsd distributions from the average structure of each of the three systems. Data shown encompass the entirety of the aggregated trajectories. The top histogram shows the difference in populations between the WT (black), 2DOR without riboflavin (sky blue), and 2DOR with the manually placed riboflavin (red). The bottom histogram shows the rmsd populations between WT (black), 2DOR-OG without riboflavin (light purple), and 2DOR-OG with the manually placed riboflavin (blue). The minor population of the WT structure at 2 Å is a slightly more compressed G-quadruplex.

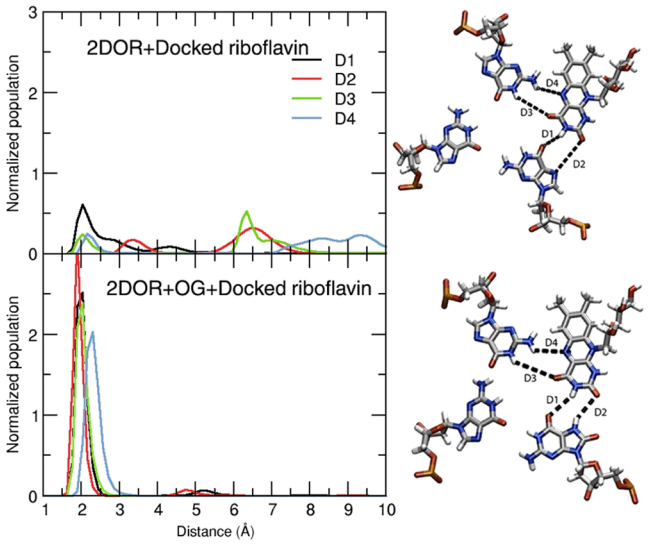

Figure 4. Distance population analysis of four distances of interest using entire aggregated trajectories. 2DOR with a docked riboflavin sequence is shown on top and 2DOR-OG with a docked riboflavin sequence is shown on the bottom. The first tetrads of the 2DOR sequence (top) and 2DOR-OG sequence (bottom) are shown to indicate distances of interest; these images were taken from starting structures, prior to equilibration.

with an abasic site and with an abasic site and an oxidized base. Due to the nature of the G-quadruplexes, it was plausible that the structures in simulation could unfold completely; however, we did not find this to be an issue. Rather, when comparing the WT system to damaged structures, we observed that the guanine tetrads retain their expected tertiary structure, at least on the simulation timescale of ∼4.5 μs, but with differences in fluctuations and structural deviations. These fluctuations extend beyond the damaged bases, as expected, to occur throughout the structure. Both the 2DOR (abasic) and 2DOR-OG (abasic and OG) structures deviate from the WT structure by ∼1.2−1.6 Å (Table 1). The two modified structures (2DOR and 2DOR-OG) are more similar to one another than their WT counterpart, with a less than 1 Å difference. For perspective, the native G-quadruplex structures only deviate ∼0.1−0.4 Å between replicas. With the addition of a docked riboflavin complex in the cavity formed by the presence of the 2-deoxyribose in position 3, we observed different effects.

The 2DOR system with the manually docked riboflavin showed increased structural deviations when compared to the WT and 2DOR structures (Figure 3). The data suggest that when riboflavin binds, the G-quadruplex structure is not as well maintained. Visual inspection of the trajectories showed riboflavin stacking in a duplex-like fashion, sitting in the abasic site as intended, and moving from the abasic site to stack on top of G11. Conversely, docking riboflavin with the 2DOR-OG-damaged G-quadruplex increases the top G-tetrad stability when compared to WT (Table 1 and Figure 3). However, the riboflavin and 2DOR-OG complex deviate more from the WT structure than they do from each other (Figure 3). This observation is likely due to the observation that riboflavin perturbs the size of the tetrad. In the WT structure, the average C1 to C1 distance between all adjacent guanines in the first tetrad is 11.6 Å (±0.2). However, in the 2DOR-OG + riboflavin simulation, only the average C1−C1 distance between G11 and the OG-modified base (residue 7) remains close to the WT with 11.7 Å (±0.2). The average C1−C1 distance between 2DOR (residue 3) and the OG-modified guanine (residue 7) decreases to 10.8 Å (±2), probably from the increased interactions between OG and riboflavin, as described later in the paper. To compensate for this change, the average C1−C1 distance between 2DOR (residue 3) and G15 is increased to 17.4 Å (±1), and the average C1−C1 distance between G11 and G15 is 12 Å (±1). Thus, the presence of riboflavin and its interactions shift the tetrad so that it is unable to match that of the native G-quadruplex structure (Figure S1).

Abasic, Oxidized Structures Remain Closer to the Native G-Quadruplex State Due to Interactions with Riboflavin. Our next step was to observe the interactions between the G-quadruplex and the manually docked riboflavin molecule. We selected four key atoms on the riboflavin, H17, O18, O15, and N13, to monitor their distance at four atoms on the 2DOR sequence, specifically for the residue@atom name pairs: G7@O6, G7@N7, G15@H1, and G15@H21. For the 2DOR-OG sequence, the same four atoms were chosen on riboflavin, but their distances were calculated to OG@O17, OG@H37, G15@H1, and G15@H21, respectively. A tetrad with residue labels can be found in Figure S2. Distances can be visualized in Figure 4. From this analysis, we can observe that riboflavin extensively samples the entire G-quadruplex in the 2DOR structure (Figure 4). Contrastingly, we see that riboflavin remains docked throughout the aggregated 2DOR-OG trajectories, until the end. Upon further analysis, we observe that the riboflavin undocks itself in the last 2 μs of one of our five replicas but remains docked for the other four (Figure S3).

https://doi.org/10.1021/acs.biochem.1c00598
Biochemistry 2022, 61, 265−275

Table 2. Hydrogen Bond Analysis Using the Entire Aggregated Trajectories[a]

2DOR + docked				2DOR-OG + docked			
acceptor	donorH	donor	%	acceptor	donorH	donor	%
2DOR@O3	RF@H48	RF@O47	25.5	OG@O17	RF@H17	RF@N16	70.2
G15@O6	RF@H46	RF@O45	16.0	G4@OP2	RF@H44	RF@O43	41.7
G7@O6	RF@H17	RF@N16	15.9	2DOR@O3	RF@H48	RF@O47	33.8
T2@OP1	RF@H48	RF@O47	12.1	2DOR@O3	RF@H46	RF@O45	27.8
2DOR@O3	RF@H42	RF@O41	09.2	2DOR@O2	RF@H48	RF@O47	14.0

[a]The acceptor column refers to the residue name and number with the acceptor atom after the @ symbol. The donorH column specifies the hydrogen while the donor column specifies the heavy atom involved in hydrogen bonding. The percentage column refers to the percentage of total frames in which the particular bond is present. Only the top five populated bonds for each system are shown. RF refers to riboflavin. A molecular graphic of riboflavin with the atoms involved in hydrogen bonding labeled can be seen below (Figure 5). OP1 and OP2 refer to the oxygens bonded to the phosphate of the DNA backbone but not involved in the phosphodiester bonds.

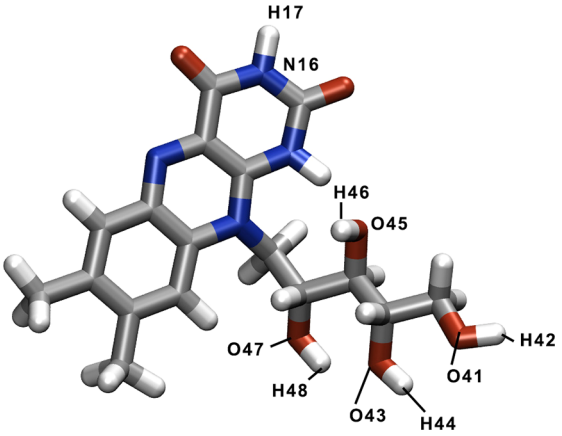

Figure 5. Molecular graphic of riboflavin with atoms involved with hydrogen bonding labeled. Atoms O47 and H48, O45 and H46, N16 and H17, and O41 and H42 are the atoms that hydrogen bond with the most frequencies in the 2DOR + riboflavin system. Atoms N16 and H17, O43 and H44, O47 and H48, and O45 and H46 are the atoms that are involved with the most hydrogen bonding in the 2DOR-OG with riboflavin system. Exact percentages of their involvement can be seen in Table 2.

Hydrogen bond analysis supported the hypothesis that the riboflavin binds with OG (Table 2). Here, we observe the function of 2-deoxyribose is to provide a space not only for riboflavin docking but for stability as well, as seen in hydrogen bonding with both the 2DOR and 2DOR-OG sequences for about 25% of the populations (Figure 5). We see that OG at O17 is involved in hydrogen bonding in 70% of the frames, providing strong evidence for the role that OG plays in this stabilization. O17 is the additional oxygen attached to C8 of the guanine base that creates OG. Visualization of the O17 and its proximity to riboflavin can be found in Figure S1. Binding energy analysis with MM-PBSA methods[52] for each sequence was performed using every 1000th frame extracted from all the sampled data (refer to the Methods for details). Binding energies from each system were subtracted from the same sequence without a docked riboflavin to produce the $\Delta\Delta G$ (Figure 6). The tetrad, defined as residues G3, G7, G11, and G15 or G7, G11, and G15 with riboflavin, showed an approximate binding energy of −4.1 kcal/mol for the 2DOR and −9.1 kcal/mol for the 2DOR-OG sequences. Each of the binding energies was broken down to account for single residue interactions. For the 2DOR sequence, −1.5 kcal/mol was contributed from G7, −2.1 from G11, and −0.1 from G15. For the 2DOR-OG sequence, the contributions were −5.7 from OG, −0.3 from G11, and −3.0 from G15. This could be from hydrogen bonding between OG and G15 that pulls the nucleobases closer together and creates a distance with G11,

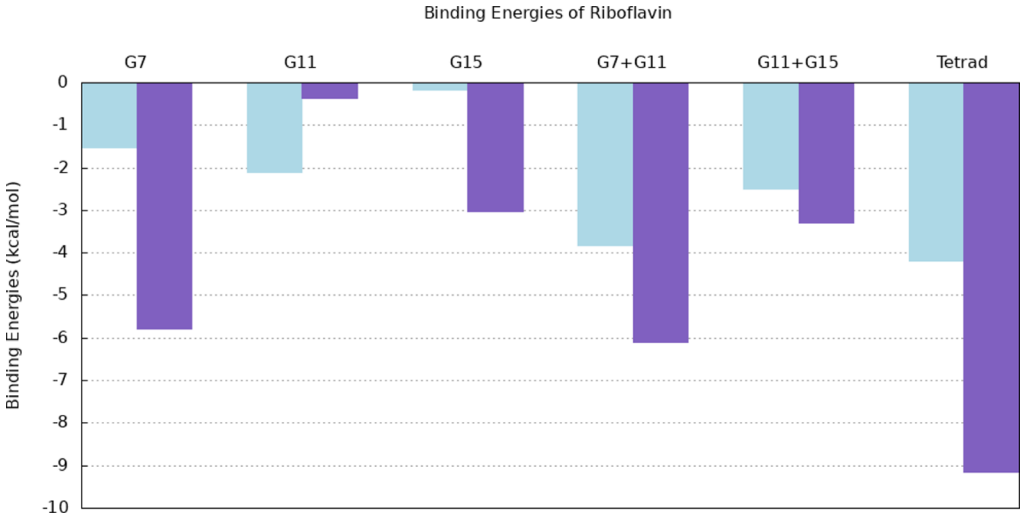

Figure 6. Binding energies (kcal/mol) of riboflavin with 2DOR + docked (blue) and 2DOR-OG + docked (purple) sequences. Binding energies estimated by the program MMPBSA were subtracted from a reference structure of each mutation without a docked riboflavin to produce the $\Delta\Delta G$ (eq 2).

https://doi.org/10.1021/acs.biochem.1c00598
Biochemistry 2022, 61, 265−275

Table 3. Hydrogen Bond Analysis Using the Entire Aggregated Trajectories[a]

2DOR + guanine				2DOR-OG + guanine			
acceptor	donorH	donor	%	acceptor	donorH	donor	%
G7@O6	GUA@H4	GUA@N5	67.6	OG@O17	GUA@H4	GUA@N5	84.9
G4@OP2	GUA@H5	GUA@N3	35.7	G4@OP2	GUA@H5	GUA@N3	57.5
G7@N7	GUA@H2	GUA@N1	28.2	T2@OP1	GUA@H1	GUA@N1	16.5
G7@N7	GUA@H1	GUA@N1	23.9	T2@OP1	GUA@H2	GUA@N1	15.1
G4@OP1	GUA@H5	GUA@N3	13.6	G4@OP1	GUA@H5	GUA@N3	11.3

[a]The acceptor column refers to the residue name and number with the involved atom specified after the @ symbol. The donorH column specifies the hydrogen while the donor column specifies the heavy atom involved in the hydrogen bonding. The percentage column refers to the percentage of total frames in which the particular bond is present. Only the top five populated bonds for each system are shown. GUA refers to the guanine. OP1 and OP2 refer to the oxygens bonded to the phosphate of the DNA backbone but not involved in the phosphodiester bonds. The molecular graphic of a guanine base with the atoms involved in hydrogen bonding labeled can be found below (Figure 7).

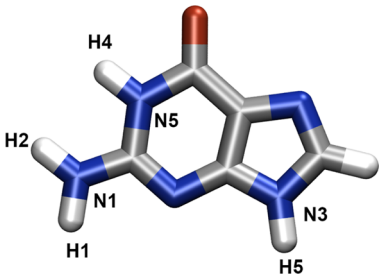

Figure 7. Molecular graphic of a free guanine base with atoms involved with hydrogen bonding labeled. Atoms N5 and H5, N3 and H5, N1 and H2, and N3 and H5 are the atoms that hydrogen bond with the most frequencies in the 2DOR + guanine system. Atoms N5 and H4, N3 and H5, N1 and H1, and N3 and H5 are the atoms that are involved with the most hydrogen bonding in the 2DOR-OG with guanine system. Exact percentages of their involvement can be seen in Table 3.

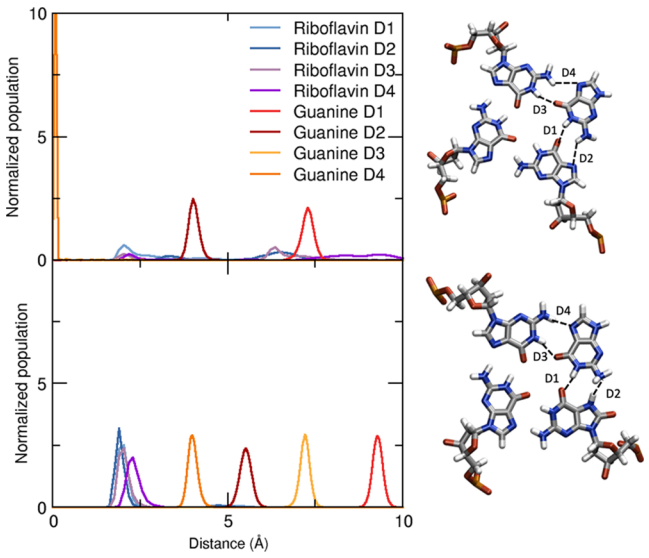

Figure 8. Distance population analysis of four distances of interest using entire aggregated trajectories. The 2DOR sequence is shown on top and the 2DOR-OG sequence is shown at the bottom. Distances shown are between riboflavin (blues and purples) or guanine (reds and oranges) and two of the residues in the first tetrad. The first tetrads of the 2DOR sequence (top) and 2DOR-OG sequence (bottom) are shown with guanine to indicate the selected distances of interest. Key distances for riboflavin can be seen in Figure 4.

resulting in a lower energetic contribution from G11 to the tetrad stability. A full breakdown of the approximate binding energies with riboflavin can be found in the Supporting Information (Tables S1 and S2).

Guanine Remains Docked in the Abasic Site in the Absence of an OG Base. To study the differences between the binding affinity of riboflavin and a guanine base, we compared the hydrogen bonding and binding energies from our previous studies to that of a docked free-floating guanine. In the initial comparison of the structures through root mean square deviation (rmsd), we observe minor differences between the structures and riboflavin or guanine ligands (Table S3). This observation forced us to take a deeper look into the specific interactions of each ligand and the structure. A hydrogen bond analysis of the guanine with the 2DOR sequence showed interactions with G7, the adjacent guanine, and with the backbone of G4 from the tetrad below (Table 3). These interactions were similar to an evaluation of the hydrogen bonding of the guanine in the native structure (Table S3). Further, a comparison of the guanine docked in the 2DOR-OG sequence identified interactions with the OG base at O17 at close to 85% of the frames. Interestingly, we identified interactions with the backbones of G4 and T2, a base from the loop sequence. These interactions between guanine and the bases of the G-quadruplex loop likely account for the perceived stabilization and decreased fluctuations of the structure (Figure 7).

A distance analysis of guanine in the abasic site supported what was observed with the hydrogen bonding data. In the 2DOR sequence, guanine remained bound and close to G7 and G11. Distances 3 and 4 were less than 1 Å from the tetrad and remained there for the entirety of the simulation (Figure 8). In contrast, riboflavin, shown in blue, which never remained docked was explored along with the entire G-quadruplex structure during the simulation. In the 2DOR-OG simulation, we see that guanine does remain in the same position throughout the simulation. However, it stays at a distance much farther from G7 and G11 than riboflavin. This observation complements that guanine in the 2DOR-OG structure interacts with non-tetrad bases than those of the first tetrad. The steric clash of the added oxygen in the OG base makes the vacancy less favorable for docking with guanine, which pushes the free base to interact with other parts of the structure. With the repulsion of the OG base, guanine not only increased in movements but also rotated its position within the vacancy, creating large differences between adjacent distances (D1 and D2, D3 and D4) (Figure S4). This is in contrast to riboflavin, which creates multiple hydrogen bonds with the top tetrad bases and remains closely docked. When breaking down the binding interactions, we further support our structural

https://doi.org/10.1021/acs.biochem.1c00598
Biochemistry 2022, 61, 265−275

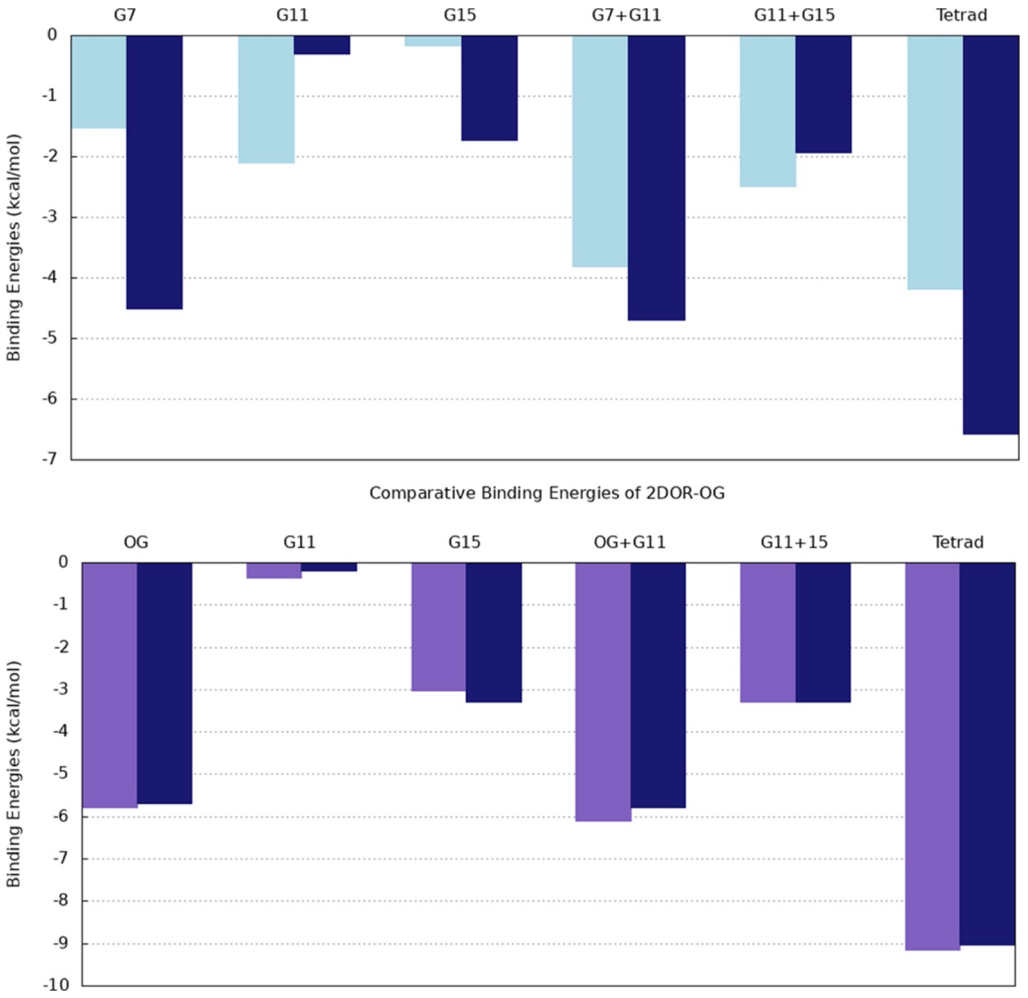

Figure 9. Comparison of the approximate binding energies of riboflavin and guanine with 2DOR (top) and 2DOR-OG (bottom) sequences. Energies calculated by the MM-PBSA methodology were subtracted from a reference structure of each mutation without a docked riboflavin to produce the $\Delta\Delta G$ (eq 2). Riboflavin is depicted in the lighter color of each graph, while guanine is depicted in dark blue.

Table 4. Comparing Approximate Binding Energies of Riboflavin and Guanine with 2DOR (Abasic) and 2DOR-OG (Abasic with Oxoguanine) Sequences[a]

2DOR			2DOR-OG		
	riboflavin	guanine		riboflavin	guanine
receptor(s)	$\Delta\Delta G$ (kcal/mol)	$\Delta\Delta G$ (kcal/mol)	receptor(s)	$\Delta\Delta G$ (kcal/mol)	$\Delta\Delta G$ (kcal/mol)
G7	−1.5	−4.5	OG	−5.8	−5.7
G11	−2.1	−0.3	G11	−0.3	−0.1
G15	−0.1	−1.7	G15	−3.0	−3.3
G7 & G11	−3.8	−4.7	OG & G11	−6.1	−5.8
G11 & G15	−2.5	−1.9	G11 & G15	−3.3	−3.3
tetrad	−4.2	−6.6	tetrad	−9.2	−9.0

[a]Energies calculated by the program MMPBSA.py were subtracted from a reference structure of each mutation without a docked riboflavin to produce the $\Delta\Delta G$ (eq 2).

observations. Guanine is more favorable in the 2DOR tetrad, with a $\Delta\Delta G$ of −6.5 kcal/mol compared to that of riboflavin with a $\Delta\Delta G$ of −4.1 kcal/mol. This can be broken down as −4.5 kcal/mol contributed by G7, −0.3 kcal/mol by G11, and −1.7 kcal/mol by G15. The large free energy contribution of G7 is expected when compared to the hydrogen bonding analysis, which shows the multiple hydrogen bonds between guanine and G7. In the 2DOR-OG sequence, guanine and riboflavin appear extremely comparable with contributions in the tetrad with −9.1 kcal/mol from riboflavin and −9.0 kcal/mol from guanine. The breakdown by residue looks similar as well with −5.6 kcal/mol contributed by OG, −0.1 kcal/mol by G11, and −3.2 kcal/mol by G15 (Figure 9 and Table 4). This similarity between the free energies of the ligands is related to the fact that both ligands can hydrogen bond with the OG. A full breakdown of the approximate binding energies with guanine can be found in the Supporting Information (Tables S1 and S2). In addition, the free energy profile was calculated

https://doi.org/10.1021/acs.biochem.1c00598
Biochemistry 2022, 61, 265−275

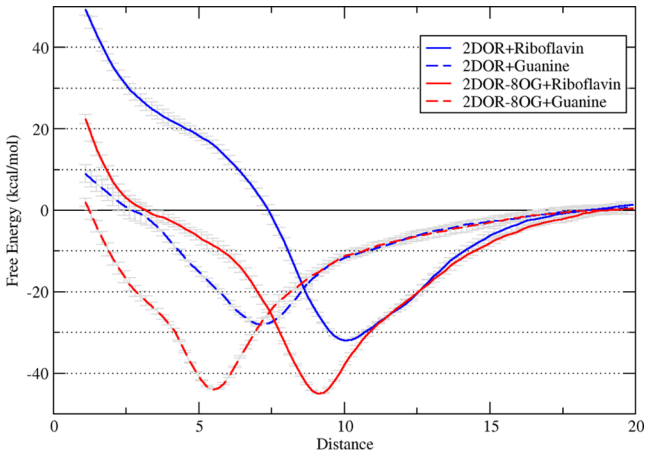

Figure 10. Free energy profiles from the umbrella sampling simulations using a distance restraint as the reaction coordinate between the center of mass of the first tetrad (residues 7, 11, and 15) and the center of mass of either the guanine or riboflavin molecule depending on the system. The profile is the average of five independent runs per window; the standard deviation is represented by the gray error bars.

using umbrella sampling at various distances from the center of mass of the top tetrad (Figure 10). The results of these calculations showed the most energetically favorable system to be the 2DOR-OG with riboflavin at a distance of ∼8 Å from the center of the tetrad. This was followed by 2DOR-OG with guanine at a much shorter distance of ∼5.5 Å from the center of the top tetrad. The 2DOR system with guanine showed a smaller energetic minimum at close to 7 Å from the center of the tetrad. This contrasts with the larger, but farther minimum of 2DOR with riboflavin 10 Å from the center. At this distance, riboflavin is strongly interacting with the backbone molecules OP1 and OP2 of the G4 residue. An image depicting this interaction can be found in the Supporting Information (Figure S5).

Riboflavin Has Not Yet Been Observed to Spontaneously Bind into the Abasic Site in Unbiased Simulations. Analysis of 640 μs of the aggregated trajectory for each of the 2DOR and 2DOR-OG systems failed to show spontaneous docking of riboflavin. Riboflavin readily explores all areas surrounding the G-quadruplex with preference to stacking on the top and bottom tetrads (Figure 11). Although previously we have seen spontaneous ligand binding to DNA, including intercalation,[46,54] sieving through the calculated trajectories, we observe riboflavin closing in on the abasic site,

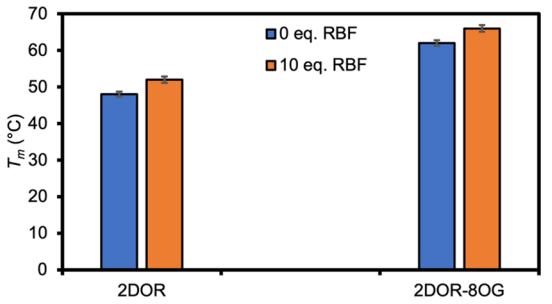

Figure 12. Melting temperatures of the 2DOR and 2DOR-8OG G-quadruplexes both in the absence of and with 10 equiv of riboflavin (RBF). An example of the melting curve used to determine T_m can be found in the Supporting Information (Figure S6).

but no spontaneous triad binding event to form the intact tetrad was found. While it is still plausible that unbiased riboflavin could in time dock the G-quadruplex, it was not observed on the time scale of these simulations. It is also possible that we did not observe a docking event due to the strong π stacking of the riboflavin over the tetrad. Discrepancies in over-stacking have been documented in the AMBER force fields.[55]

Experimental Exploration of Vacancy-Containing G-Quadruplex Structures in the Presence of Riboflavin. In tandem with the computation work performed, the interaction between riboflavin and the abasic, oxidized G-quadruplex structures was studied. The stability of the G-quadruplex with and without riboflavin was first analyzed through thermal melting (T_m). This showed that in both the 2DOR and 2DOR-8OG G-quadruplexes, the melting temperature was increased by 4 °C when in the presence of 10 equiv of riboflavin (Figure 12). This is similar to literature values that show that guanosine monophosphate can increase the melting temperature of an abasic, parallel G-quadruplex by 5 °C.[30] While an increase in the stability of the 2DOR-8OG was expected based on the computational work, the increase in T_m of the 2DOR G-quadruplex in the presence of riboflavin was not expected. This increase could be an artifact of the riboflavin stacking with the structure rather than docking in the vacancy site as predicted.

We then set out to study experimentally the docking of riboflavin to a vacancy site in the G-quadruplex with OG in K^+-containing solutions. The DNA strand was synthesized with the modifications to create the vacancy. The strand was folded in a K^+ solution, and then the CD spectra were recorded before and after the addition of 10 equiv of riboflavin (Figure 13A). The CD spectra both presented with λ_{max} around 263 nm,

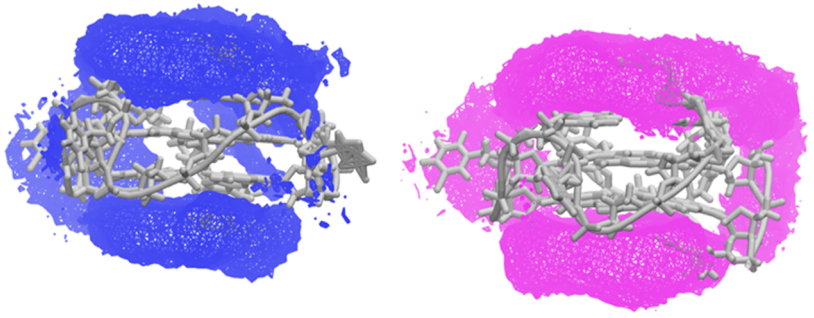

Figure 11. Grid density analysis for the 2DOR (blue) and 2DOR-OG (pink) G-quadruplexes with free riboflavin represented with the same isodensity value (using the mesh representation). The CPPTRAJ analysis script used is available in the Supporting Information.

https://doi.org/10.1021/acs.biochem.1c00598
Biochemistry 2022, 61, 265−275

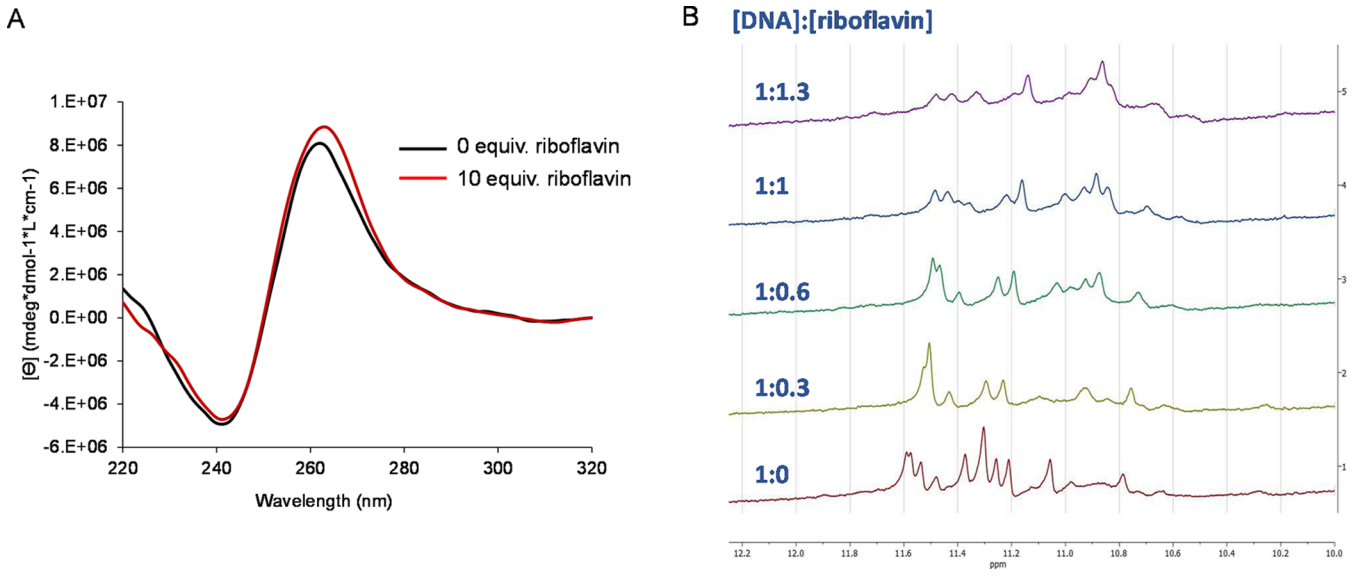

Figure 13. Monitoring riboflavin docking with the OG vacancy-containing G-quadruplex using CD spectroscopy and NMR. (A) CD spectra before and after the addition of 10 equiv of riboflavin. (B) ^{1}H NMR monitoring imino protons as riboflavin was titrated into the G-quadruplex.

indicating a parallel-stranded fold consistent with the simulations before and after riboflavin addition. Next, a titration of riboflavin with the abasic site-containing G-quadruplex was monitored using ^{1}H NMR while focusing on the Hoogsteen imino region of the spectra. Before the addition of riboflavin, 10 imino peaks were observed, consistent with a G-quadruplex bearing a vacancy, as predicted by the simulations. As riboflavin was added from 0.5 to 1.25 equiv, the imino proton intensities decreased down to 7 and shifted, suggesting an interaction that is less defined than before riboflavin addition (Figure 13B). The simulations nicely explain why the ^{1}H NMR data report on a less stable fold because the calculations found riboflavin docking results in a less ordered structure than the vacancy. This final experiment supports the findings from the MD simulations, showing that riboflavin can dock into the vacancy of the OG G-quadruplex while causing additional disruptions to the structure that did not exist before docking.

CONCLUSIONS

The G-quadruplex structure is innately susceptible to oxidative damage leading to its degradation.[16,17,21] In this combined simulation and experimental work, we examined the ability of riboflavin to bind to and stabilize damaged G-quadruplex structures. Through extensive MD simulation, we determined that riboflavin could stabilize the G-quadruplex depending on the type of damage. When the G-quadruplex contains an abasic-site (as shown by the 2DOR sequence), we saw no stabilization effect from riboflavin. However, when an OG was placed adjacent to the abasic site, we observed a general stabilization of the complex. The riboflavin no longer explored the entirety of the structure, as was observed with the 2DOR sequence; rather it remained docked in the abasic site. This is likely due in part to the hydrogen bonding between the riboflavin and O17 of OG. When comparing the results of riboflavin in the MD simulation with that of guanine, we observe the opposite trend. Guanine hydrogen bonds and remains closely docked in the tetrad with an abasic site present. However, with the presence of both an abasic site and an adjacent OG base, the guanine is pushed farther outside of the tetrad and interacts with other parts of the G-quadruplex structure, such as the loop. The docking of riboflavin to the damaged G-quadruplex experimentally validated the finding that the CD spectrum was that of a parallel-stranded G-quadruplex before and after riboflavin addition. The disruption of the OG vacancy G-quadruplex upon riboflavin docking found in the MD simulations was consistent with the ^{1}H NMR studies that found riboflavin docking disrupted the imino pattern diagnostic of G-quadruplex folding. These studies lead us to conclude that riboflavin is able to stabilize an oxidized G-quadruplex structure in the abasic site.

ASSOCIATED CONTENT

Supporting Information

The Supporting Information is available free of charge at https://pubs.acs.org/doi/10.1021/acs.biochem.1c00598.

Visualization of key interactions and phenomena, more expansive MMPBSA breakdown, the riboflavin mol2 file, 2DOR parameters, and selected examples of the inputs required to reproduce the analysis using CPPTRAJ (PDF)

AUTHOR INFORMATION

Corresponding Author

Thomas E. Cheatham, III − *Department of Medicinal Chemistry, College of Pharmacy, University of Utah, Salt Lake City, Utah 84112, United States;* orcid.org/0000-0003-0298-3904; Email: tec3@utah.edu

Authors

Rodrigo Galindo-Murillo − *Department of Medicinal Chemistry, College of Pharmacy, University of Utah, Salt Lake City, Utah 84112, United States*

Lauren Winkler − *Department of Medicinal Chemistry, College of Pharmacy, University of Utah, Salt Lake City, Utah 84112, United States;* orcid.org/0000-0002-9439-3225

Jingwei Ma − *Department of Chemistry, University of Utah, Salt Lake City, Utah 84112-0850, United States*

Fatjon Hanelli − *Department of Chemistry, University of Utah, Salt Lake City, Utah 84112-0850, United States*
Aaron M. Fleming − *Department of Chemistry, University of Utah, Salt Lake City, Utah 84112-0850, United States;* orcid.org/0000-0002-2000-0310
Cynthia J. Burrows − *Department of Chemistry, University of Utah, Salt Lake City, Utah 84112-0850, United States;* orcid.org/0000-0001-7253-8529

Complete contact information is available at: https://pubs.acs.org/10.1021/acs.biochem.1c00598

Author Contributions

§R.G.-M. and L.W. contributed equally to this work.

Notes

The authors declare no competing financial interest.

Data Availability: Pre-processed trajectories of all the simulations (no solvent molecules, imaged and RMS fit), topology files, and analysis scripts are available for download at the URL: https://amber.utah.edu/DNA-dynamics/riboflavin/.

■ ACKNOWLEDGMENTS

This research was enabled by the Blue Waters sustained petascale computing project (NSF ACI-15155 PRAC OCI-1036208), the NSF Extreme Science and Engineering Discovery Environment[56] (XSEDE, OCI-1053575), NSF (CHE-1808475), and allocation MCA01S027P and the Center for High Performance Computing at the University of Utah. Funding from the National Institutes of Health and R-01 GM-081411 is acknowledged.

■ REFERENCES

(1) Gellert, M.; Lipsett, M. N.; Davies, D. R. Helix Formation by Guanylic Acid. *Proc. Natl. Acad. Sci. U.S.A.* **1962**, *48*, 2013−2018.
(2) Ou, T.-m.; Lu, Y.-j.; Tan, J.-h.; Huang, Z.-s.; Wong, K.-Y.; Gu, L.-q. G-Quadruplexes: Targets in Anticancer Drug Design. *ChemMedChem* **2008**, *3*, 690−713.
(3) Vannutelli, A.; Belhamiti, S.; Garant, J.-M.; Ouangraoua, A.; Perreault, J.-P. Where Are G-Quadruplexes Located in the Human Transcriptome? *NAR: Genomics Bioinf.* **2020**, *2*, lqaa035.
(4) Ghosh, A.; Largy, E.; Gabelica, V. DNA G-Quadruplexes for Native Mass Spectrometry in Potassium: A Database of Validated Structures in Electrospray-Compatible Conditions. *Nucleic Acids Res.* **2021**, *49*, 2333−2345.
(5) Lipps, H. J.; Rhodes, D. G-Quadruplex Structures: In Vivo Evidence and Function. *Trends Cell Biol.* **2009**, *19*, 414−422.
(6) Webba da Silva, M. Geometric Formalism for DNA Quadruplex Folding. *Chem.—Eur. J.* **2007**, *13*, 9738−9745.
(7) Karsisiotis, A. I.; O'Kane, C.; Webba da Silva, M. DNA Quadruplex Folding Formalism − A Tutorial on Quadruplex Topologies. *Methods* **2013**, *64*, 28−35.
(8) Artandi, S. E.; DePinho, R. A. Telomeres and Telomerase in Cancer. *Carcinogenesis* **2010**, *31*, 9−18.
(9) Zvereva, M. I.; Shcherbakova, D. M.; Dontsova, O. A. Telomerase: Structure, Functions, and Activity Regulation. *Biochemistry* **2010**, *75*, 1563−1583.
(10) Zahler, A. M.; Williamson, J. R.; Cech, T. R.; Prescott, D. M. Inhibition of Telomerase by G-Quartet DMA Structures. *Nature* **1991**, *350*, 718−720.
(11) Rocca, R.; Moraca, F.; Costa, G.; Nadai, M.; Scalabrin, M.; Talarico, C.; Distinto, S.; Maccioni, E.; Ortuso, F.; Artese, A.; Alcaro, S.; Richter, S. N. Identification of G-Quadruplex DNA/RNA Binders: Structure-Based Virtual Screening and Biophysical Characterization. *Biochim. Biophys. Acta, Gen. Subj.* **2017**, *1861*, 1329−1340.
(12) Siddiqui-Jain, A.; Grand, C. L.; Bearss, D. J.; Hurley, L. H. Direct Evidence for a G-Quadruplex in a Promoter Region and Its Targeting with a Small Molecule to Repress c-MYC Transcription. *Proc. Natl. Acad. Sci. U.S.A.* **2002**, *99*, 11593−11598.
(13) Neidle, S. Quadruplex Nucleic Acids as Novel Therapeutic Targets. *J. Med. Chem.* **2016**, *59*, 5987−6011.
(14) Saito, I.; Takayama, M.; Sugiyama, H.; Nakatani, K.; Tsuchida, A.; Yamamoto, M. Photoinduced DNA Cleavage via Electron Transfer: Demonstration That Guanine Residues Located 5' to Guanine Are the Most Electron-Donating Sites. *J. Am. Chem. Soc.* **1995**, *117*, 6406−6407.
(15) Steenken, S.; Jovanovic, S. V. How Easily Oxidizable Is DNA? One-Electron Reduction Potentials of Adenosine and Guanosine Radicals in Aqueous Solution. *J. Am. Chem. Soc.* **1997**, *119*, 617−618.
(16) Fleming, A. M.; Burrows, C. J. Interplay of Guanine Oxidation and G-Quadruplex Folding in Gene Promoters. *J. Am. Chem. Soc.* **2020**, *142*, 1115−1136.
(17) Fleming, A. M.; Burrows, C. J. G-Quadruplex Folds of the Human Telomere Sequence Alter the Site Reactivity and Reaction Pathway of Guanine Oxidation Compared to Duplex DNA. *Chem. Res. Toxicol.* **2013**, *26*, 593−607.
(18) Cui, L.; Ye, W.; Prestwich, E. G.; Wishnok, J. S.; Taghizadeh, K.; Dedon, P. C.; Tannenbaum, S. R. Comparative Analysis of Four Oxidized Guanine Lesions from Reactions of DNA with Peroxynitrite, Singlet Oxygen, and γ-Radiation. *Chem. Res. Toxicol.* **2013**, *26*, 195−202.
(19) Fleming, A. M.; Burrows, C. J. 8-Oxo-7,8-Dihydroguanine, Friend and Foe: Epigenetic-like Regulator versus Initiator of Mutagenesis. *DNA Repair* **2017**, *56*, 75−83.
(20) Hao, W.; Qi, T.; Pan, L.; Wang, R.; Zhu, B.; Aguilera-Aguirre, L.; Radak, Z.; Hazra, T. K.; Vlahopoulos, S. A.; Bacsi, A.; Brasier, A. R.; Ba, X.; Boldogh, I. Effects of the Stimuli-Dependent Enrichment of 8-Oxoguanine DNA Glycosylase1 on Chromatinized DNA. *Redox Biol.* **2018**, *18*, 43−53.
(21) Seifermann, M.; Epe, B. Oxidatively Generated Base Modifications in DNA: Not Only Carcinogenic Risk Factor but Also Regulatory Mark? *Free Radicals Biol. Med.* **2017**, *107*, 258−265.
(22) Cogoi, S.; Ferino, A.; Miglietta, G.; Pedersen, E. B.; Xodo, L. E. The Regulatory G4 Motif of the Kirsten Ras (KRAS) Gene Is Sensitive to Guanine Oxidation: Implications on Transcription. *Nucleic Acids Res.* **2018**, *46*, 661−676.
(23) Gedik, C. M.; Gedik, C. M.; Collins, A. Establishing the Background Level of Base Oxidation in Human Lymphocyte DNA: Results of an Interlaboratory Validation Study. *FASEB J.* **2005**, *19*, 82−84.
(24) Mangerich, A.; Knutson, C. G.; Parry, N. M.; Muthupalani, S.; Ye, W.; Prestwich, E.; Cui, L.; McFaline, J. L.; Mobley, M.; Ge, Z.; Taghizadeh, K.; Wishnok, J. S.; Wogan, G. N.; Fox, J. G.; Tannenbaum, S. R.; Dedon, P. C. Infection-Induced Colitis in Mice Causes Dynamic and Tissue-Specific Changes in Stress Response and DNA Damage Leading to Colon Cancer. *Proc. Natl. Acad. Sci. U.S.A.* **2012**, *109*, E1820−E1829.
(25) Esposito, V.; Martino, L.; Citarella, G.; Virgilio, A.; Mayol, L.; Giancola, C.; Galeone, A. Effects of Abasic Sites on Structural, Thermodynamic and Kinetic Properties of Quadruplex Structures. *Nucleic Acids Res.* **2010**, *38*, 2069−2080.
(26) Lindahl, T. DNA Repair Enzymes. *Annu. Rev. Biochem.* **1982**, *51*, 61−87.
(27) Školáková, P.; Bednářová, K.; Vorlíčková, M.; Sagi, J. Quadruplexes of Human Telomere DG3(TTAG3)3 Sequences Containing Guanine Abasic Sites. *Biochem. Biophys. Res. Commun.* **2010**, *399*, 203−208.
(28) Virgilio, A.; Petraccone, L.; Esposito, V.; Citarella, G.; Giancola, C.; Galeone, A. The Abasic Site Lesions in the Human Telomeric Sequence d[TA(G3T2A)3G3]: A Thermodynamic Point of View. *Biochim. Biophys. Acta, Gen. Subj.* **2012**, *1820*, 2037−2043.
(29) Wang, K.-B.; Dickerhoff, J.; Wu, G.; Yang, D. PDGFR-β Promoter Forms a Vacancy G-Quadruplex That Can Be Filled in by DGMP: Solution Structure and Molecular Recognition of Guanine Metabolites and Drugs. *J. Am. Chem. Soc.* **2020**, *142*, 5204−5211.

(30) Li, X.-m.; Zheng, K.-w.; Zhang, J.-y.; Liu, H.-h.; He, Y.-d.; Yuan, B.-f.; Hao, Y.-h.; Tan, Z. Guanine-Vacancy−Bearing G-Quadruplexes Responsive to Guanine Derivatives. *Proc. Natl. Acad. Sci. U.S.A.* **2015**, *112*, 14581−14586.
(31) Li, Q.; Fei, Y.; Gao, L.; Yu, Y.; Zhou, Y.; Ye, T.; Zhou, X.-S.; Shao, Y.; Yin, Z.-Z. G-Quadruplex DNA with an Apurinic Site as a Soft Molecularly Imprinted Sensing Platform. *Anal. Chem.* **2018**, *90*, 5552−5556.
(32) Incles, C. M.; Schultes, C. M.; Kempski, H.; Koehler, H.; Kelland, L. R.; Neidle, S. A G-Quadruplex Telomere Targeting Agent Produces P16-Associated Senescence and Chromosomal Fusions in Human Prostate Cancer Cells. *Mol. Cancer Ther.* **2004**, *3*, 1201−1206.
(33) Riou, J. F.; Guittat, L.; Mailliet, P.; Laoui, A.; Renou, E.; Petitgenet, O.; Mégnin-Chanet, F.; Hélène, C.; Mergny, J. L. Cell Senescence and Telomere Shortening Induced by a New Series of Specific G-Quadruplex DNA Ligands. *Proc. Natl. Acad. Sci. U.S.A.* **2002**, *99*, 2672−2677.
(34) Burger, A. M.; Dai, F.; Schultes, C. M.; Reszka, A. P.; Moore, M. J.; Double, J. A.; Neidle, S. The G-Quadruplex-Interactive Molecule BRACO-19 Inhibits Tumor Growth, Consistent with Telomere Targeting and Interference with Telomerase Function. *Cancer Res.* **2005**, *65*, 1489−1496.
(35) Chen, Z.-F.; Qin, Q.-P.; Qin, J.-L.; Zhou, J.; Li, Y.-L.; Li, N.; Liu, Y.-C.; Liang, H. Water-Soluble Ruthenium(II) Complexes with Chiral 4-(2,3-Dihydroxypropyl)-Formamide Oxoaporphine (FOA): In Vitro and in Vivo Anticancer Activity by Stabilization of G-Quadruplex DNA, Inhibition of Telomerase Activity, and Induction of Tumor Cell Apoptosis. *J. Med. Chem.* **2015**, *58*, 4771−4789.
(36) Xin, Z.; Pu, L.; Gao, W.; Wang, Y.; Wei, J.; Shi, T.; Yao, Z.; Guo, C. Riboflavin Deficiency Induces a Significant Change in Proteomic Profiles in HepG2 Cells. *Sci. Rep.* **2017**, *7*, 45861.
(37) Dennington, R.; Keith, T. A.; Millam, J. M. *GaussView*; Semichem Inc.: Shawnee Mission, KS, 2016.
(38) Zhao, Y.; Truhlar, D. G. The M06 Suite of Density Functionals for Main Group Thermochemistry, Thermochemical Kinetics, Noncovalent Interactions, Excited States, and Transition Elements: Two New Functionals and Systematic Testing of Four M06-Class Functionals and 12 Other Functionals. *Theor. Chem. Acc.* **2008**, *120*, 215−241.
(39) McLean, A. D.; Chandler, G. S. Contracted Gaussian Basis Sets for Molecular Calculations. I. Second Row Atoms, Z=11−18. *J. Chem. Phys.* **1980**, *72*, 5639−5648.
(40) Wang, J.; Wolf, R. M.; Caldwell, J. W.; Kollman, P. A.; Case, D. A. Development and Testing of a General Amber Force Field. *J. Comput. Chem.* **2004**, *25*, 1157−1174.
(41) Do, N. Q.; Phan, A. T. Monomer-Dimer Equilibrium for the 5′-5′ Stacking of Propeller-Type Parallel-Stranded G-Quadruplexes: NMR Structural Study. *Chem.—Eur. J.* **2012**, *18*, 14752−14759.
(42) Galindo-Murillo, R.; Robertson, J. C.; Zgarbová, M.; Šponer, J.; Otyepka, M.; Jurečka, P.; Cheatham, T. E. Assessing the Current State of Amber Force Field Modifications for DNA. *J. Chem. Theory Comput.* **2016**, *12*, 4114−4127.
(43) Cheng, X.; Kelso, C.; Hornak, V.; de los Santos, C.; Grollman, A. P.; Simmerling, C. Dynamic Behavior of DNA Base Pairs Containing 8-Oxoguanine. *J. Am. Chem. Soc.* **2005**, *127*, 13906−13918.
(44) Jorgensen, W. L.; Chandrasekhar, J.; Madura, J. D.; Impey, R. W.; Klein, M. L. Comparison of Simple Potential Functions for Simulating Liquid Water. *J. Chem. Phys.* **1983**, *79*, 926−935.
(45) Joung, I. S.; Cheatham, T. E. Determination of Alkali and Halide Monovalent Ion Parameters for Use in Explicitly Solvated Biomolecular Simulations. *J. Phys. Chem. B* **2008**, *112*, 9020−9041.
(46) Galindo-Murillo, R.; García-Ramos, J. C.; Ruiz-Azuara, L.; Cheatham, T. E.; Cortés-Guzmán, F. Intercalation Processes of Copper Complexes in DNA. *Nucleic Acids Res.* **2015**, *43*, 5364−5376.
(47) Berendsen, H. J. C.; Postma, J. P. M.; van Gunsteren, W. F.; DiNola, A.; Haak, J. R. Molecular Dynamics with Coupling to an External Bath. *J. Chem. Phys.* **1984**, *81*, 3684−3690.
(48) Pearlman, D. A.; Case, D. A.; Caldwell, J. W.; Ross, W. S.; Cheatham, T. E.; DeBolt, S.; Ferguson, D.; Seibel, G.; Kollman, P. AMBER, a Package of Computer Programs for Applying Molecular Mechanics, Normal Mode Analysis, Molecular Dynamics and Free Energy Calculations to Simulate the Structural and Energetic Properties of Molecules. *Comput. Phys. Commun.* **1995**, *91*, 1−41.
(49) Case, D. A.; Cheatham, T. E.; Darden, T.; Gohlke, H.; Luo, R.; Merz, K. M.; Onufriev, A.; Simmerling, C.; Wang, B.; Woods, R. J. The Amber Biomolecular Simulation Programs. *J. Comput. Chem.* **2005**, *26*, 1668−1688.
(50) Roe, D. R.; Cheatham, T. E. Parallelization of CPPTRAJ Enables Large Scale Analysis of Molecular Dynamics Trajectory Data. *J. Comput. Chem.* **2018**, *39*, 2110−2117.
(51) *Gaussian 09*; Gaussian, Inc.: Wallingford, CT, 2016.
(52) Miller, B. R.; McGee, T. D.; Swails, J. M.; Homeyer, N.; Gohlke, H.; Roitberg, A. E. MMPBSA.Py: An Efficient Program for End-State Free Energy Calculations. *J. Chem. Theory Comput.* **2012**, *8*, 3314−3321.
(53) Fleming, A. M.; Zhu, J.; Ding, Y.; Visser, J. A.; Zhu, J.; Burrows, C. J. Human DNA Repair Genes Possess Potential G-Quadruplex Sequences in Their Promoters and 5′-Untranslated Regions. *Biochemistry* **2018**, *57*, 991−1002.
(54) Galindo-Murillo, R.; Winkler, L.; García-Ramos, J. C.; Ruiz-Azuara, L.; Cortés-Guzmán, F.; Cheatham, T. E. Ancillary Ligand in Ternary CuII Complexes Guides Binding Selectivity toward Minor-Groove DNA. *J. Phys. Chem. B* **2020**, *124*, 11648−11658.
(55) Pérez, A.; Luque, F. J.; Orozco, M. Frontiers in Molecular Dynamics Simulations of DNA. *Acc. Chem. Res.* **2012**, *45*, 196−205.
(56) Towns, J.; Cockerill, T.; Dahan, M.; Foster, I.; Gaither, K.; Grimshaw, A.; Hazlewood, V.; Lathrop, S.; Lifka, D.; Peterson, G. D.; Roskies, R.; Scott, J. R.; Wilkins-Diehr, N. XSEDE: Accelerating Scientific Discovery. *Comput. Sci. Eng.* **2014**, *16*, 62−74.

https://doi.org/10.1021/acs.biochem.1c00598
Biochemistry 2022, 61, 265−275